Molecular Composition of Oxygenated Organic Molecules and Their Contributions to Organic Aerosol in Beijing

Wang, Yonghong

2022-01-18

http://hdl.handle.net/10138/344293
https://doi.org/10.1021/acs.est.1c05191

unspecified
submittedVersion

Molecular composition of oxygenated organic molecules and their contributions to organic aerosol in Beijing

Yonghong Wang[1,2,5,*], Petri Clusius[2], Chao Yan[2], Kaspar Dällenbach[2], Rujing Yin[3], Mingyi Wang[4], Xu-Cheng He[2], Biwu Chu[5], Yiqun Lu[6], Lubna Dada[2], Juha Kangasluoma[1,2], Pekka Rantala[2], Chenjuan Deng[3], Zhuohui Lin[1], Weigang Wang[7], Lei Yao[2], Xiaolong Fan[1], Wei Du[2], Jing Cai[2], Liine Heikkinen[2], Yee Jun Tham[2], Qiaozhi Zha[2], Zhenghao Ling[2], Heikki Junninen[2,10], Tuukka Petäjä[2], Maofa Ge[7], Yuesi Wang[8], Hong He[5], Douglas R. Worsnop[9], Veli-Matti Kerminen[2], Federico Bianchi[1,2], Lin Wang[6], Jingkun Jiang[3, *], Yongchun Liu[1, *], Michael Boy[2], Mikael Ehn[2], Neil M. Donahue[4] and Markku Kulmala[1,2, *]

[1]Aerosol and Haze Laboratory, Beijing Advanced Innovation Center for Soft Matter Science and Engineering, Beijing University of Chemical Technology, Beijing 100089, China

[2]Institute for Atmospheric and Earth System Research / Physics, Faculty of Science, University of Helsinki, Helsinki 00560, Finland

[3] School of Environment, Tsinghua University, Beijing 100084, China

[4]Carnegie Mellon University Center for Atmospheric Particle Studies, 5000 Forbes Ave, Pittsburgh Pennsylvania, 15213, USA.

[5] Research Center for Eco-Environmental Sciences, Chinese Academy of Sciences, Beijing 100085, China

[6]Department of Environmental Science & Engineering, Fudan University, Shanghai 200438, China

[7]Institute of Chemistry, Chinese Academy of Sciences, Beijing 100029, China

[8] Institute of Atmospheric Physics, Chinese Academy of Sciences, Beijing 100029, China

[9]Aerodyne Research Inc., Billerica, Massachusetts 01821, USA.

[10] Institute of Physics, University of Tartu, Tartu 50090, Estonia

*Corresponding authors:

Markku Kulmala: markku.kulmala@helisnki.fi

Yongchun Liu: liuyc@buct.edu.cn

Jingkun Jiang: jiangjk@mail.tsinghua.edu.cn

Yonghong Wang: yonghongwang@rcees.ac.cn

Abstract

The understanding at a molecular level of ambient secondary organic aerosol (SOA) formation is hampered by poorly constrained formation mechanisms and insufficient analytical methods. Especially in developing countries, SOA related haze is a great concern due to its significant effects on climate and human health. We present simultaneous measurements of gas-phase volatile organic compounds (VOC), oxygenated organic molecules (OOM), and particle-phase SOA in Beijing. We show that condensation of the measured OOM explains 26-39% of the organic aerosol mass growth, with the contribution of OOM to SOA enhanced during severe haze episodes. Our novel results provide a quantitative molecular connection from anthropogenic emissions, to condensable organic oxidation product vapors, their concentration in particle-phase SOA, and ultimately to haze formation.
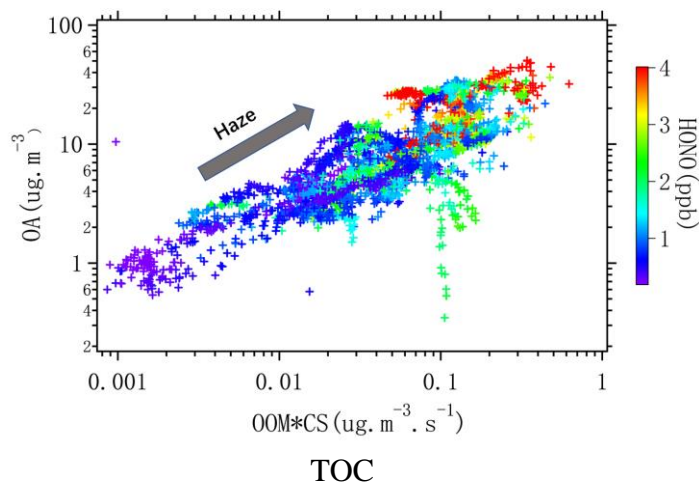
Synopsis

The work represents an advance in the understanding of the gap between organic vapors and organic aerosol that plays a vital role during haze.

Keywords

air pollution, organic aerosol, haze, oxygenated organic molecules, volatility

TOC

Introduction

Air pollution in China has caused great concern due to its effect on human health and climate [1-4], although recent studies have revealed a remarkable reduction of particulate matter (PM) over eastern China since 2013 [5, 6]. Secondary organic aerosol (SOA) is an important component of fine particulate matter and thus haze [7]. On a global scale, gas-to-particle partitioning of low volatility organic compounds (LVOCs) is considered to be the main formation pathway of SOA, while aqueous-phase formation of LVOCs is a significant supplement to the global SOA burden [8-12]. Especially in megacities of China, intense production of SOA is considered to be responsible for severe haze formation [13-15]. Abundant organic vapors from anthropogenic emissions are oxidized by hydroxyl radicals (OH), nitrate radicals (NO_3), ozone (O_3) and chlorine atoms (Cl), and subsequently influenced by nitrogen oxides (NO_x), sulfur dioxide (SO_2) and ammonia (NH_3). The chemical system is extremely complicated, especially because of cross reactions between different peroxy radicals. It is difficult to elucidate urban organic aerosol formation at a molecular level, even in a well-controlled smog chamber [16-18].

Volatility of atmospheric organic vapors determines the preference of vapors for the gas or particle phase [19, 20]. Organic volatility is closely related to functional groups and oxidation state. Recently, formation of highly oxygenated organic molecules via autoxidation has been proposed as an important route for condensable vapor formation [21]. The process is characterized by multiple intramolecular H atom shifts in peroxy radicals, each followed by rapid oxygen addition to form multifunctional peroxy radicals with a high oxidation extent [21-24]. However, autoxidation may be limited in urban areas due to the high concentration of nitric oxide (NO) [25]. Although the majority of peroxy radicals react with NO by forming alkoxy radicals and NO_2, the rapid reaction of NO with peroxy radicals will terminate the autoxidation process by forming closed-shell products. These products are less oxygenated and therefore semi-volatile (SVOCs), though LVOCs and also extremely low volatile organic compounds (ELVOC) are still formed; consequently, this lowers the yield of LVOCs, which play a vital role in growth of newly formed particles [17, 21]. However, multiple generations of oxidation may also be important under highly oxidizing conditions [26, 27].

Online detection of highly oxygenated organic molecules at the sub-ppt level only recently became possible with the development of the NO_3-CI-APi-ToF, which is a novel instrument for measurement of gas-phase sulfuric acid and highly oxygenated organic molecules based on the selective and sensitive clustering of nitrate anions with hydroxyl and hydroperoxyl groups [21, 28]. However, as yet there have been few deployments of the NO_3-CI-APi-ToF in the urban atmosphere to measure oxygenated organic compounds and their role in aerosol formation and growth [29-31]. Organic aerosol associated with haze formation in Chinese megacities have been studied extensively with advanced online mass-spectrometer technology utilizing electron ionization [32]. However, this approach only provides aerosol fragments and elementary information of bulk organic aerosol composition; knowledge about organic-aerosol composition at the molecular level is still limited.

Materials and method

Sampling site

The measurements were conducted between 3-30 March 2018 on the rooftop of a university building at the west campus of the Beijing University of Chemical Technology (39.95°N, 116.31°E). This station is located about 150 m away from the nearest road (Zizhuyuan road) and 500 m away from the West Third Ring Road. The station is surrounded by commercial properties and residential dwellings and is thus representative of a typical urban environment.

Measurement of OOM and calibration

Oxidized organic molecules are measured by a chemical ionization long time-of-flight mass spectrometer (LToF-CIMS, Aerodyne Research, Inc.) equipped with a nitrate chemical ionization source [28]. Ambient air is drawn into the ionization source through a stainless-steel tube with a length of 1.6 m and a diameter of 3/4 inch. A mixture of a 3 mL min^{-1} ultrahigh purity nitrogen flow containing nitric acid and a 20 L min^{-1} pure air flow supplied by a zero-air generator (Aadco 737, USA), together as a sheath flow, is guided through a PhotoIonizer (Model L9491, Hamamatsu, Japan) to produce nitrate reagent ions. This sheath flow is then introduced into a co-axial laminar flow reactor concentric to the sample flow. Nitrate ions are pushed to the sample flow layer by an electric field and subsequently charge analyte molecules. Throughout the campaign, the sample flow rate is kept at 8.8 L min^{-1}, out of which about 0.8 L min^{-1} is drawn through the pinhole into the TOF module and the rest is extracted by vacuum. We use 1.1×10^{10} molecule cm^{-3} as the calibration coefficient after taking into account the diffusion loss of OOM in the 1.6m sampling line.

Estimation of organic vapor concentration includes two steps. Firstly, a mass-dependent transmission correction is performed. Such mass-dependency is instrument-specific and is influenced by many instrumental parameters. This transmission bias is determined by depleting the primary ion with a series of perfluorinated acids and comparing the primary ion signal depletion with the product signal increase (which would match for equivalent transmission efficiency). The detailed method was described in a previous study [33]. Second, we apply the calibration coefficient determined for sulfuric acid to estimate the organic vapor concentration.

For the OOM measured here, we assume that NO_3^- clustering has the same rate coefficient as the sulfuric acid ion transfer reaction (i.e. both are collision limited), which is supported for ELVOC and ULVOC multifunctional organics in the literature [21]. Because the OOM form clusters with NO_3^-, we have removed the NO_3^- from all of the reported ion masses and chemical formulas reported here.

Measurement of organic aerosol, calibration and sources apportionment with PMF

Online Time-of-Flight Aerosol Chemical Speciation Monitor (ToF-ACSM, equipped with a standard vaporizer) observations were conducted at the BUCT station from February 21 to April 7, 2018, equipped with a PM$_{2.5}$ lens [34]. The non-refractory fraction of fine-particle mass concentrations (NR-PM$_{2.5}$, including organics, sulfate, nitrate, ammonium, and chloride) were obtained by the ToF-ACSM standard data analysis software (Tofware) within Igor Pro (Wavemetrics). The ToF-ACSM was regularly calibrated (ionization efficiency) and relative ionization efficiency (RIE) of NH$_4$ (3.76) and SO$_4$ (0.88) were experimentally determined by using nebulizing aqueous solutions of pure NH$_4$NO$_3$ and pure (NH$_4$)$_2$SO$_4$ into the ToF-ACSM. Default relative ionization efficiency (RIE) values were used for organics (1.4), nitrate (1.1), and chloride (1.3). The organic mass spectra from the ToF-ACSM were analyzed by positive matrix factorization (PMF) to identify and quantify the potential sources of organic aerosol (OA). We solved the PMF by the multi-linear engine (ME-2) algorithm implemented within the toolkit SoFi, Source Finder[35]. Exploratory unconstrained PMF runs separated primary OA (POA) from traffic (HOA), and cooking (COA), a component representing residential heating (mixture of biomass burning, BBOA, and coal combustion, CCOA), and a component representing secondary OA (SOA).

MALTE-box model

158 Measured particle size distributions from the SMPS were used in the zero-dimensional model
159 MALTE-box, which simulates atmospheric chemistry and aerosol dynamics [36]. Since the
160 chemical structure and therefore the reaction rates of the measured OOM compounds were not
161 known, the chemistry module in MALTE-box was bypassed and the aerosol dynamics was
162 applied using measured oxygenated organic molecules. To calculate the condensation and
163 evaporation of the vapors to and from the particle phase, the model uses their molecular mass and
164 saturation vapor pressure, calculated using a parametrization by Donahue et al. (2012) and
165 experimentally confirmed by Wang et al. (2020). The evaporation and condensation are explicitly
166 calculated for each gas compound and particle diameter using Fuchs-Sutugin corrected collision
167 rate and the Kelvin and Raoult's effect. Particle size evolution is then due to particle growth and
168 coagulation.

169 To focus the simulations on the effect of the measured OOM to the mass increase in the particle
170 phase, the model was run in a constricted mode so that every 10 minutes the measured particle
171 size distribution was used to initialize the model distribution. The measured OOM were then
172 allowed to condense to (or evaporate from) the particles, according to their saturation vapor
173 pressures and concentrations. From the modeled output the flux of the vapors to particle phase
174 was calculated using the time in between the consecutive model initializations. In this way, we
175 were able to use the measured conditions as closely as possible and assess the mass flux at any
176 particular moment.

177

178 **Results and discussion**

179 Molecular characterization of OOM

180 In Fig. 1(a, b) we present molecular characteristics of oxygenated organic molecules (OOM)
181 measured in Beijing by an NO_3-CI-APi-ToF; however, we cannot classify all of these OOMs as
182 highly oxygenated organic molecules (HOM) [17]. Most of these OOM have molecular masses
183 between 200-450 amu, with carbon numbers between 5 and 18. Molecules with one or two
184 nitrogen atoms predominate, and the highest signals are from nitrophenol related compounds, e.g.,
185 $C_6H_5NO_3$ and $C_7H_7NO_3$. The measured total OOM concentration on average is around 1–2 x 10^9
186 molecules cm^{-3}, which is 10 times higher than the values measured in a boreal forest region
187 dominated by monoterpene emissions[37]. The OOM concentrations are highest during haze periods
188 (with $PM_{2.5} > 75$ µg m^{-3}), which may be explained by high concentrations of total aromatic
189 volatile organic compounds (the summed concentrations of benzene, toluene, trimethylbenzene,
190 ethyl toluene, propyl benzene and diethyl benzene) as shown in extend Fig. S1 (b). To elucidate
191 the evolution of OOM and aromatic precursors, as well as nitrous acid (HONO), we show the
192 diurnal variation of these parameters along with boundary layer height (see extend Fig. S1). These
193 compounds are largely mediated by boundary layer processes; high concentrations of OOM,
194 aromatic vapors and organic aerosol usually occurred during nighttime with a shallow boundary
195 layer.

196 In the urban atmosphere, OH and NO_3 are the dominant oxidants for most aromatic compounds;
197 once the oxidants attack the aromatic ring, autoxidation can be triggered [16, 24]. However, high
198 concentrations of NO in ambient Beijing can terminate autoxidation and lead to the formation of
199 compounds containing multiple nitrogen atoms [26, 27, 38]. Noting that these closed-shell products
200 still are reactive with OH and NO_3, multiple generations of oxidation may occur in the
201 atmosphere as well as in chamber studies[27]. We observed compounds containing several nitrogen
202 atoms in ambient Beijing, as depicted in Fig.1(a), consistent with both autoxidation and multi-
203 generation chemistry.

204 Overall, the oxidation chemistry can be represented by the oxidation state of carbon [39]. As shown
205 in Fig. 1(b), the average oxidation state of carbon in the ambient vapors measured with the NO_3^-
206 CI-APi-ToF tends to decrease with increasing carbon number. The highest carbon oxidation state
207 occurs in molecules with 5 carbons, with formulas $C_5H_9NO_6$ and $C_5H_{10}N_2O_8$, which are related
208 multi-generation oxidation products from isoprene terminated by NO (see Extend data Fig. S3).
209 Note that the source of isoprene and monoterpenes is not only biogenic emission but also
210 emission of anthropogenic volatile chemical products [40, 41]. The carbon oxidation state presented
211 here is higher than that in the boreal forest region, which is dominated by monoterpenes with
212 lower NO_x concentrations [42]. The conditions with high NO concentration and strong atmospheric
213 oxidation capacity favoring multi-generation reactions lead to a high carbon oxidation state in
214 Beijing, while first-generation products are the dominant products in the boreal forest region [21].
215 This may be the main reason for the large discrepancy in carbon oxidation state between the two
216 environments.

217 The oxidized vapors we measure with the NO_3-CI-APi-ToF are a key bridge connecting aromatic
218 precursors emitted in the urban atmosphere to oxygenated organic aerosol and thus haze
219 formation. As shown in Fig.2 (a), the variation of OOM shows a good correlation with aromatic
220 VOC during both haze and clean periods (defined by a high or low condensation sink). Aromatic
221 VOC emissions are predominately on-road vehicle exhaust [40]. The formation of secondary
222 organic aerosol from anthropogenic VOC has been the subject of numerous chamber studies. In
223 general, long-chain alkanes and aromatic compounds (benzene, toluene, etc.) are considered to be
224 the main precursors of anthropogenic SOA [43]. Given the large emission sources of anthropogenic
225 VOC and their fate in ambient Beijing, these aromatic VOC should be a large source of the OOM
226 observed here [44]. OOM condensation may in turn be the main source of SOA. Fig.2 (b) shows that
227 there is a strong correlation between OOM and the oxidized organic aerosol factor (OOA)
228 measured by a time of flight aerosol chemical speciation monitor (ToF-ACSM), suggesting that
229 condensation of these OOM contributes to the mass of OOA. The OOA in turn constitutes the
230 majority of the OA, especially during haze events.

Contributions of OOM to PM and haze

232 The relative contribution of different OOMs to SOA formation depends on their driving forces for
233 net condensation, largely constrained by vapor concentration and volatility [10, 45, 46]. We estimate
234 the volatility of observed OOMs using a combination of two quantitatively confirmed VBS
235 parameterizations to reflect the contribution of aging (multi-generation OH oxidation) [45, 46] and
236 autoxidation [17] to the OOM formation, respectively (see Fig. S4) [26]. Because the volatility of
237 OOMs varies by more than 10 decades, we group them together within a volatility basis set
238 (VBS) (Fig. 3).

239 In general, OOMs during haze periods have a similar volatility distribution to that during non-
240 haze periods, but with notably higher concentrations in all volatility bins (Fig. 3A). The ultra-low,
241 extremely low and low-volatility organic compounds (ULVOCs, ELVOCs and LVOCs) have
242 sufficiently low saturation vapor pressures to be efficient condensable material; the semivolatile
243 organic compounds (SVOCs) contribute to particle mass via equilibrium gas-particle partitioning.
244 Intermediate volatile organic compounds (IVOCs), however, have a minor direct contribution to
245 SOA formation in this study, although the most abundant OOMs were phenolic compounds such
246 as nitrophenol. We integrate OOMs from the lowest volatility bin to $C^* \leq 10^{0.5}$ µg m^{-3}, to show
247 the tentative abundance of condensable vapors (shaded area in Fig. 3B). OOMs potentially
248 formed from the aging pathway and the autoxidation pathway are separated by a dashed dividing
249 line (Fig. 3B and Fig. S4). Interestingly, during both the haze and non-haze periods, the aging
250 products dominate in the ULVOC range, while the autoxidation products become more abundant
251 in the ELVOC range and take over in the LVOC range. The overall increase in the tentative

condensable vapors from non-haze to haze periods is approximately 40 % in mass (Fig. 3C). Moreover, the OOMs in the ULVOC and ELVOC ranges rise more than those in the LVOC range, with species potentially formed from aging pathways being the major contributor. This suggests that photochemical aging might be a major process that drives the SOA formation we observe in Beijing during the observation periods.

To quantify the contribution of the measured OOM to the mass concentration of organic aerosol in PM$_{2.5}$, we estimated the contribution of OOM to the total PM$_{2.5}$ mass flux using MALTE-box (Model to predict Aerosol formation in Lower Troposphere, see Methods), which treats both gas-to-particle condensation and evaporation of OOM from particles. We restricted our analysis to periods of PM$_{2.5}$ growth so that we could constrain the mass flux via the measured growth rate. As shown in Fig. 4(a), LVOC and ELVOC dominated aerosol mass growth, consistent with being saturated as observed. Overall, 26% and 39% of the organic-aerosol mass increase is explained by condensation of OOM during non-haze and haze conditions, respectively (see Fig.4c). This corresponds to 9 % and 23 % of the total PM$_{2.5}$ mass increase. The uncertainties of these values due to uncertain volatility are limited, as shown in Table S1. The additional organic growth implied by the difference between the measured (ToF-ACSM) organic mass growth and the calculated OOM condensation rate is likely do to some combination of aqueous condensed-phase chemistry and equilibrium partitioning of unmeasured SVOC, where the nitrate CI-API-ToF is less sensitive[47]. As listed in Table S2, the compounds with the largest contributions to the flux were $C_{10}H_{14}O_9N$, $C_{10}H_{15}O_8N$, and $C_{10}H_{16}O_9N_2$, which may arise from monoterpene oxidation, and $C_{14}H_{15}O_8N$, $C_{12}H_{20}O_8N_2$, and $C_8H_{13}O_{11}$, which may arise from aromatic oxidation. Most of the mass flux is driven by numerous products likely associated with a variety of aromatic precursors.

The higher contribution of OOM to PM$_{2.5}$ and organic-aerosol mass during the haze periods is associated with a higher condensation sink and higher OOM concentrations, which may enhance the gas to particle conversion. As we show in Fig. 4 (b), the empirical relationship between mass fluxes and condensation sink is non-linear, indicating enhanced vapor condensation to preexisting aerosol as haze grows more severe.

Although our study provides a quantified relationship between oxygenated organic vapor molecules in the gas phase and organic aerosol in the particle phase, uncertainties and limitations still exist. First, we quantify all OOM based on the sulfuric acid calibration, but the binding affinity of the nitrate anion to organic functional groups may vary, adding uncertainty. However, for many highly functionalized OOM, the same kinetic limit that applies to sulfuric acid is likely to hold. Second, we estimate volatility based on measured molecular composition rather than measuring the exact vapor pressure of individual OOM species. Therefore, the parameterized volatility distribution will lead to uncertainty in estimated partitioning. However, the measured volatility of aromatic oxidation products matches this parameterization to within a factor of 10 [26]. Finally, advection and external sources and sinks are not explicitly considered in the box model, and a fraction of organic aerosol in the urban atmosphere is from transport of upwind region, with aging processes occurring within the plume, while the formation of OOM vapors is likely to be local.

Quantification of specific chemical oxidation products from various organic precursors and their contribution to SOA formation during haze episodes is essential to understand haze formation. Those molecular formation mechanisms of SOA, and thereby haze, are far from completely elucidated in megacities like Beijing. Our results reveal a substantial pool of oxygenated organic vapors that can condense to particles and explain 26-39% of organic-aerosol mass growth. We show that most of these OOM are nitrogen containing compounds, suggesting that multi-step

oxidation processes are essential in the urban atmosphere. In particular, these OOM contribute more during high PM loading conditions, due to both increased OOM concentrations and condensation sink, which facilitates gas to particle conversion processes. Noting that the nitrate chemical ionization scheme is only sensitive to a subset of compounds, e.g., organic molecules with -OOH groups, -OH groups and/or -NO$_2$ groups, other quantitative chemical ionization methods should be employed to develop a comprehensive picture of oxygenated volatile organic compounds. Regardless, our current results could provide a substantial number of oxygenated VOCs for air quality models that are currently not treated.

Supporting Information

Details on the measurement of VOC and HONO, data sources of NO$_2$, O$_3$, SO$_2$ and PM$_{2.5}$, measurement of mixing layer height, calculation method of condensation sink, estimation of the volatility of OOMs and extended figures and tables.

Author Contributions: Y.W. designed the research. Y.W., C.Y., K.D., R.Y., X.H., B.C., J.K., P.R., C.D., W.W., L.H., H.J., F.B., L.W., J.J., and Y.L. conducted the measurements. P.C. and M.B performed box model simulation. Y.W., L.D., Z.L., L.Y., X.F., W.D., J.C., Y.T., T.P., M.G., Y.W., H.H., D.W., V.K., M.E. and N.D. contributed to the scientific discussion. Y.W. wrote the main manuscript with contributions from N.D. M.W. and P. C. **Competing interests:** The authors declare no competing interest. **Data and materials availability:** Data and materials are available upon contacting the corresponding authors

Reference

1.   Lelieveld, J.; Evans, J. S.; Fnais, M.; Giannadaki, D.; Pozzer, A., The contribution of outdoor air pollution sources to premature mortality on a global scale. *Nature* **2015,** *525*, 367.
2.   Ding, A. J.; Huang, X.; Nie, W.; Sun, J. N.; Kerminen, V. M.; Petäjä, T.; Su, H.; Cheng, Y. F.; Yang, X. Q.; Wang, M. H.; Chi, X. G.; Wang, J. P.; Virkkula, A.; Guo, W. D.; Yuan, J.; Wang, S. Y.; Zhang, R. J.; Wu, Y. F.; Song, Y.; Zhu, T.; Zilitinkevich, S.; Kulmala, M.; Fu, C. B., Enhanced haze pollution by black carbon in megacities in China. *Geophysical Research Letters* **2016,** *43*, (6), 2873-2879.
3.   Zhang, Q.; Jiang, X.; Tong, D.; Davis, S. J.; Zhao, H.; Geng, G.; Feng, T.; Zheng, B.; Lu, Z.; Streets, D. G.; Ni, R.; Brauer, M.; van Donkelaar, A.; Martin, R. V.; Huo, H.; Liu, Z.; Pan, D.; Kan, H.; Yan, Y.; Lin, J.; He, K.; Guan, D., Transboundary health impacts of transported global air pollution and international trade. *Nature* **2017,** *543*, (7647), 705-709.
4.   An, Z.; Huang, R. J.; Zhang, R.; Tie, X.; Li, G.; Cao, J.; Zhou, W.; Shi, Z.; Han, Y.; Gu, Z.; Ji, Y., Severe haze in northern China: A synergy of anthropogenic emissions and atmospheric processes. *Proceedings of the National Academy of Sciences of the United States of America* **2019,** *116*, (18), 8657-8666.
5.   Zhang, Q.; Zheng, Y.; Tong, D.; Shao, M.; Wang, S.; Zhang, Y.; Xu, X.; Wang, J.; He, H.; Liu, W.; Ding, Y.; Lei, Y.; Li, J.; Wang, Z.; Zhang, X.; Wang, Y.; Cheng, J.; Liu, Y.; Shi, Q.;

Yan, L.; Geng, G.; Hong, C.; Li, M.; Liu, F.; Zheng, B.; Cao, J.; Ding, A.; Gao, J.; Fu, Q.; Huo, J.; Liu, B.; Liu, Z.; Yang, F.; He, K.; Hao, J., Drivers of improved PM2.5 air quality in China from 2013 to 2017. *Proceedings of the National Academy of Sciences of the United States of America* **2019,** *116*, (49), 24463-24469.

6.   Wang, Y.; Gao, W.; Wang, S.; Song, T.; Gong, Z.; Ji, D.; Wang, L.; Liu, Z.; Tang, G.; Huo, Y.; Tian, S.; Li, J.; Li, M.; Yang, Y.; Chu, B.; Petäjä, T.; Kerminen, V.-M.; He, H.; Hao, J.; Kulmala, M.; Wang, Y.; Zhang, Y., Contrasting trends of PM2.5 and surface-ozone concentrations in China from 2013 to 2017. *National Science Review* **2020,** *7*, (8), 1331-1339.

7.   Huang, R. J.; Zhang, Y.; Bozzetti, C.; Ho, K. F.; Cao, J. J.; Han, Y.; Daellenbach, K. R.; Slowik, J. G.; Platt, S. M.; Canonaco, F.; Zotter, P.; Wolf, R.; Pieber, S. M.; Bruns, E. A.; Crippa, M.; Ciarelli, G.; Piazzalunga, A.; Schwikowski, M.; Abbaszade, G.; Schnelle-Kreis, J.; Zimmermann, R.; An, Z.; Szidat, S.; Baltensperger, U.; El Haddad, I.; Prevot, A. S., High secondary aerosol contribution to particulate pollution during haze events in China. *Nature* **2014,** *514*, (7521), 218-22.

8.   Hallquist, M.; Wenger, J. C.; Baltensperger, U.; Rudich, Y.; Simpson, D.; Claeys, M.; Dommen, J.; Donahue, N. M.; George, C.; Goldstein, A. H.; Hamilton, J. F.; Herrmann, H.; Hoffmann, T.; Iinuma, Y.; Jang, M.; Jenkin, M. E.; Jimenez, J. L.; Kiendler-Scharr, A.; Maenhaut, W.; McFiggans, G.; Mentel, T. F.; Monod, A.; Prévôt, A. S. H.; Seinfeld, J. H.; Surratt, J. D.; Szmigielski, R.; Wildt, J., The formation, properties and impact of secondary organic aerosol: current and emerging issues. *Atmos. Chem. Phys.* **2009,** *9*, (14), 5155-5236.

9.   Jimenez, J. L.; Canagaratna, M. R.; Donahue, N. M.; Prevot, A. S. H.; Zhang, Q.; Kroll, J. H.; DeCarlo, P. F.; Allan, J. D.; Coe, H.; Ng, N. L.; Aiken, A. C.; Docherty, K. S.; Ulbrich, I. M.; Grieshop, A. P.; Robinson, A. L.; Duplissy, J.; Smith, J. D.; Wilson, K. R.; Lanz, V. A.; Hueglin, C.; Sun, Y. L.; Tian, J.; Laaksonen, A.; Raatikainen, T.; Rautiainen, J.; Vaattovaara, P.; Ehn, M.; Kulmala, M.; Tomlinson, J. M.; Collins, D. R.; Cubison, M. J.; Dunlea, J.; Huffman, J. A.; Onasch, T. B.; Alfarra, M. R.; Williams, P. I.; Bower, K.; Kondo, Y.; Schneider, J.; Drewnick, F.; Borrmann, S.; Weimer, S.; Demerjian, K.; Salcedo, D.; Cottrell, L.; Griffin, R.; Takami, A.; Miyoshi, T.; Hatakeyama, S.; Shimono, A.; Sun, J. Y.; Zhang, Y. M.; Dzepina, K.; Kimmel, J. R.; Sueper, D.; Jayne, J. T.; Herndon, S. C.; Trimborn, A. M.; Williams, L. R.; Wood, E. C.; Middlebrook, A. M.; Kolb, C. E.; Baltensperger, U.; Worsnop, D. R., Evolution of Organic Aerosols in the Atmosphere. *Science* **2009,** *326*, (5959), 1525-1529.

10.   Riipinen, I.; Yli-Juuti, T.; Pierce, J. R.; Petäjä, T.; Worsnop, D. R.; Kulmala, M.; Donahue, N. M., The contribution of organics to atmospheric nanoparticle growth. *Nature Geoscience* **2012,** *5*, (7), 453-458.

11.   Ervens, B.; Turpin, B. J.; Weber, R. J., Secondary organic aerosol formation in cloud droplets and aqueous particles (aqSOA): a review of laboratory, field and model studies. *Atmospheric Chemistry and Physics* **2011,** *11*, (21), 11069-11102.

12.   Gkatzelis, G. I.; Papanastasiou, D. K.; Karydis, V. A.; Hohaus, T.; Liu, Y.; Schmitt, S. H.; Schlag, P.; Fuchs, H.; Novelli, A.; Chen, Q.; Cheng, X.; Broch, S.; Dong, H.; Holland, F.; Li, X.; Liu, Y.; Ma, X.; Reimer, D.; Rohrer, F.; Shao, M.; Tan, Z.; Taraborrelli, D.; Tillmann, R.; Wang, H.; Wang, Y.; Wu, Y.; Wu, Z.; Zeng, L.; Zheng, J.; Hu, M.; Lu, K.; Hofzumahaus, A.; Zhang, Y.; Wahner, A.; Kiendler-Scharr, A., Uptake of Water-soluble Gas-phase Oxidation Products Drives Organic Particulate Pollution in Beijing. *Geophysical Research Letters* **2021,** *48*, (8). e2020GL091351, https://doi.org/10.1029/2020GL091351.

13.   Huang, R.-J.; Zhang, Y.; Bozzetti, C.; Ho, K. F.; Cao, J.; Han, Y.; Daellenbach, K.; G Slowik, J.; Platt, S.; Canonaco, F.; Zotter, P.; Wolf, R.; Pieber, S.; Bruns, E.; Crippa, M.; Ciarelli, G.; Piazzalunga, A.; Schwikowski, M.; Abbaszade, G.; Prevot, A., *High secondary aerosol contribution to particulate pollution during haze events in China*. 2014; Vol. 514.

14.   Guo, S.; Hu, M.; Zamora, M. L.; Peng, J.; Shang, D.; Zheng, J.; Du, Z.; Wu, Z.; Shao, M.; Zeng, L.; Molina, M. J.; Zhang, R., Elucidating severe urban haze formation in China. *Proceedings of the National Academy of Sciences of the United States of America* **2014,** *111*, (49), 17373-8.

15.   Sun, Y.; Jiang, Q.; Wang, Z.; Fu, P.; Li, J.; Yang, T.; Yin, Y., Investigation of the sources and evolution processes of severe haze pollution in Beijing in January 2013. *Journal of Geophysical Research: Atmospheres* **2014,** *119*, (7), 4380-4398.

16.   Atkinson, R.; Arey, J., Atmospheric Degradation of Volatile Organic Compounds. *Chemical reviews* **2003,** *103*, (12), 4605-4638.

17.   Bianchi, F.; Kurten, T.; Riva, M.; Mohr, C.; Rissanen, M. P.; Roldin, P.; Berndt, T.; Crounse, J. D.; Wennberg, P. O.; Mentel, T. F.; Wildt, J.; Junninen, H.; Jokinen, T.; Kulmala, M.; Worsnop, D. R.; Thornton, J. A.; Donahue, N.; Kjaergaard, H. G.; Ehn, M., Highly Oxygenated Organic Molecules (HOM) from Gas-Phase Autoxidation Involving Peroxy Radicals: A Key Contributor to Atmospheric Aerosol. *Chemical reviews* **2019,** *119*, (6), 3472-3509.

18.   Zhang, R.; Wang, G.; Guo, S.; Zamora, M. L.; Ying, Q.; Lin, Y.; Wang, W.; Hu, M.; Wang, Y., Formation of Urban Fine Particulate Matter. *Chemical reviews* **2015,** *115*, (10), 3803-3855.

19.   Donahue, N. M.; Ortega, I. K.; Chuang, W.; Riipinen, I.; Riccobono, F.; Schobesberger, S.; Dommen, J.; Baltensperger, U.; Kulmala, M.; Worsnop, D. R.; Vehkamaki, H., How do organic vapors contribute to new-particle formation? *Faraday Discuss* **2013,** *165*, 91-104.

20.   Trostl, J.; Chuang, W. K.; Gordon, H.; Heinritzi, M.; Yan, C.; Molteni, U.; Ahlm, L.; Frege, C.; Bianchi, F.; Wagner, R.; Simon, M.; Lehtipalo, K.; Williamson, C.; Craven, J. S.; Duplissy, J.; Adamov, A.; Almeida, J.; Bernhammer, A. K.; Breitenlechner, M.; Brilke, S.; Dias, A.; Ehrhart, S.; Flagan, R. C.; Franchin, A.; Fuchs, C.; Guida, R.; Gysel, M.; Hansel, A.; Hoyle, C. R.; Jokinen, T.; Junninen, H.; Kangasluoma, J.; Keskinen, H.; Kim, J.; Krapf, M.; Kurten, A.; Laaksonen, A.; Lawler, M.; Leiminger, M.; Mathot, S.; Mohler, O.; Nieminen, T.; Onnela, A.; Petaja, T.; Piel, F. M.; Miettinen, P.; Rissanen, M. P.; Rondo, L.; Sarnela, N.; Schobesberger, S.; Sengupta, K.; Sipila, M.; Smith, J. N.; Steiner, G.; Tome, A.; Virtanen, A.; Wagner, A. C.; Weingartner, E.; Wimmer, D.; Winkler, P. M.; Ye, P.; Carslaw, K. S.; Curtius, J.; Dommen, J.; Kirkby, J.; Kulmala, M.; Riipinen, I.; Worsnop, D. R.; Donahue, N. M.; Baltensperger, U., The role of low-volatility organic compounds in initial particle growth in the atmosphere. *Nature* **2016,** *533*, (7604), 527-31.

21.   Ehn, M.; Thornton, J. A.; Kleist, E.; Sipila, M.; Junninen, H.; Pullinen, I.; Springer, M.; Rubach, F.; Tillmann, R.; Lee, B.; Lopez-Hilfiker, F.; Andres, S.; Acir, I. H.; Rissanen, M.; Jokinen, T.; Schobesberger, S.; Kangasluoma, J.; Kontkanen, J.; Nieminen, T.; Kurten, T.; Nielsen, L. B.; Jorgensen, S.; Kjaergaard, H. G.; Canagaratna, M.; Maso, M. D.; Berndt, T.; Petaja, T.; Wahner, A.; Kerminen, V. M.; Kulmala, M.; Worsnop, D. R.; Wildt, J.; Mentel, T. F., A large source of low-volatility secondary organic aerosol. *Nature* **2014,** *506*, (7489), 476-9.

22.   Jokinen, T.; Sipila, M.; Richters, S.; Kerminen, V. M.; Paasonen, P.; Stratmann, F.; Worsnop, D.; Kulmala, M.; Ehn, M.; Herrmann, H.; Berndt, T., Rapid autoxidation forms highly oxidized RO2 radicals in the atmosphere. *Angew Chem Int Ed Engl* **2014,** *53*, (52), 14596-600.

23.   Mentel, T. F.; Springer, M.; Ehn, M.; Kleist, E.; Pullinen, I.; Kurtén, T.; Rissanen, M.; Wahner, A.; Wildt, J., Formation of highly oxidized multifunctional compounds: autoxidation of peroxy radicals formed in the ozonolysis of alkenes – deduced from structure–product relationships. *Atmospheric Chemistry and Physics* **2015,** *15*, (12), 6745-6765.

24.   Crounse, J. D.; Nielsen, L. B.; Jørgensen, S.; Kjaergaard, H. G.; Wennberg, P. O., Autoxidation of Organic Compounds in the Atmosphere. *The Journal of Physical Chemistry Letters* **2013,** *4*, (20), 3513-3520.

25.   Praske, E.; Otkjær, R. V.; Crounse, J. D.; Hethcox, J. C.; Stoltz, B. M.; Kjaergaard, H. G.; Wennberg, P. O., Atmospheric autoxidation is increasingly important in urban and suburban North America. *Proceedings of the National Academy of Sciences* **2018,** *115*, (1), 64.

26.   Wang, M.; Chen, D.; Xiao, M.; Ye, Q.; Stolzenburg, D.; Hofbauer, V.; Ye, P.; Vogel, A. L.; Mauldin, R. L., 3rd; Amorim, A.; Baccarini, A.; Baumgartner, B.; Brilke, S.; Dada, L.; Dias, A.; Duplissy, J.; Finkenzeller, H.; Garmash, O.; He, X. C.; Hoyle, C. R.; Kim, C.; Kvashnin, A.; Lehtipalo, K.; Fischer, L.; Molteni, U.; Petaja, T.; Pospisilova, V.; Quelever, L. L. J.; Rissanen, M.; Simon, M.; Tauber, C.; Tome, A.; Wagner, A. C.; Weitz, L.; Volkamer, R.; Winkler, P. M.; Kirkby, J.; Worsnop, D. R.; Kulmala, M.; Baltensperger, U.; Dommen, J.; El-Haddad, I.; Donahue, N. M., Photo-oxidation of Aromatic Hydrocarbons Produces Low-Volatility Organic Compounds. *Environmental science & technology* **2020,** *54*, (13), 7911-7921.

27.   Garmash, O.; Rissanen, M. P.; Pullinen, I.; Schmitt, S.; Kausiala, O.; Tillmann, R.; Zhao, D.; Percival, C.; Bannan, T. J.; Priestley, M.; Hallquist, Å. M.; Kleist, E.; Kiendler-Scharr, A.; Hallquist, M.; Berndt, T.; McFiggans, G.; Wildt, J.; Mentel, T. F.; Ehn, M., Multi-generation OH oxidation as a source for highly oxygenated organic molecules from aromatics. *Atmospheric Chemistry and Physics* **2020,** *20*, (1), 515-537.

28.   Jokinen, T.; Sipilä, M.; Junninen, H.; Ehn, M.; Lönn, G.; Hakala, J.; Petäjä, T.; Mauldin, R. L.; Kulmala, M.; Worsnop, D. R., Atmospheric sulphuric acid and neutral cluster measurements using CI-APi-TOF. *Atmospheric Chemistry and Physics* **2012,** *12*, (9), 4117-4125.

29.   Yao, L.; Garmash, O.; Bianchi, F.; Zheng, J.; Yan, C.; Kontkanen, J.; Junninen, H.; Mazon, S. B.; Ehn, M.; Paasonen, P.; Sipilä, M.; Wang, M.; Wang, X.; Xiao, S.; Chen, H.; Lu, Y.; Zhang, B.; Wang, D.; Fu, Q.; Geng, F.; Li, L.; Wang, H.; Qiao, L.; Yang, X.; Chen, J.; Kerminen, V.-M.; Petäjä, T.; Worsnop, D. R.; Kulmala, M.; Wang, L., Atmospheric new particle formation from sulfuric acid and amines in a Chinese megacity. *Science* **2018,** *361*, (6399), 278-281.

30.   Brean, J.; Harrison, R. M.; Shi, Z.; Beddows, D. C. S.; Acton, W. J. F.; Hewitt, C. N.; Squires, F. A.; Lee, J., Observations of highly oxidized molecules and particle nucleation in the atmosphere of Beijing. *Atmospheric Chemistry and Physics* **2019,** *19*, (23), 14933-14947.

31.   Yan, C.; Yin, R.; Lu, Y.; Dada, L.; Yang, D.; Fu, Y.; Kontkanen, J.; Deng, C.; Garmash, O.; Ruan, J.; Baalbaki, R.; Schervish, M.; Cai, R.; Bloss, M.; Chan, T.; Chen, T.; Chen, Q.; Chen, X.; Chen, Y.; Chu, B.; Dällenbach, K.; Foreback, B.; He, X.; Heikkinen, L.; Jokinen, T.; Junninen, H.; Kangasluoma, J.; Kokkonen, T.; Kurppa, M.; Lehtipalo, K.; Li, H.; Li, H.; Li, X.; Liu, Y.; Ma, Q.; Paasonen, P.; Rantala, P.; Pileci, R. E.; Rusanen, A.; Sarnela, N.; Simonen, P.; Wang, S.; Wang, W.; Wang, Y.; Xue, M.; Yang, G.; Yao, L.; Zhou, Y.; Kujansuu, J.; Petäjä, T.; Nie, W.; Ma, Y.; Ge, M.; He, H.; Donahue, N. M.; Worsnop, D. R.; Veli-Matti, K.; Wang, L.; Liu, Y.; Zheng, J.; Kulmala, M.; Jiang, J.; Bianchi, F., The Synergistic Role of Sulfuric Acid, Bases, and Oxidized Organics Governing New-Particle Formation in Beijing. *Geophysical Research Letters* **2021,** *48*, (7). e2020GL091944. https://doi.org/10.1029/2020GL091944.

32.   Li, Y. J.; Sun, Y.; Zhang, Q.; Li, X.; Li, M.; Zhou, Z.; Chan, C. K., Real-time chemical characterization of atmospheric particulate matter in China: A review. *Atmospheric Environment* **2017,** *158*, 270-304.

33.   Heinritzi, M.; Simon, M.; Steiner, G.; Wagner, A. C.; Kürten, A.; Hansel, A.; Curtius, J., Characterization of the mass-dependent transmission efficiency of a CIMS. *Atmospheric Measurement Techniques* **2016,** *9*, (4), 1449-1460.

34.   Fröhlich, R.; Cubison, M. J.; Slowik, J. G.; Bukowiecki, N.; Prévôt, A. S. H.; Baltensperger, U.; Schneider, J.; Kimmel, J. R.; Gonin, M.; Rohner, U.; Worsnop, D. R.; Jayne, J. T., The ToF-ACSM: a portable aerosol chemical speciation monitor with TOFMS detection. *Atmospheric Measurement Techniques* **2013,** *6*, (11), 3225-3241.

35.   Canonaco, F.; Crippa, M.; Slowik, J. G.; Baltensperger, U.; Prévôt, A. S. H., SoFi, an IGOR-based interface for the efficient use of the generalized multilinear engine (ME-2) for the

490 source apportionment: ME-2 application to aerosol mass spectrometer data. *Atmos. Meas. Tech.*
491 **2013,** *6*, (12), 3649-3661.
492 36.   Boy, M.; Hellmuth, O.; Korhonen, H.; Nilsson, E. D.; ReVelle, D.; Turnipseed, A.;
493 Arnold, F.; Kulmala, M., MALTE – model to predict new aerosol formation in the lower
494 troposphere. *Atmos. Chem. Phys.* **2006,** *6*, (12), 4499-4517.
495 37.   Zha, Q.; Yan, C.; Junninen, H.; Riva, M.; Sarnela, N.; Aalto, J.; Quéléver, L.; Schallhart,
496 S.; Dada, L.; Heikkinen, L.; Peräkylä, O.; Zou, J.; Rose, C.; Wang, Y.; Mammarella, I.; Katul, G.;
497 Vesala, T.; Worsnop, D. R.; Kulmala, M.; Petäjä, T.; Bianchi, F.; Ehn, M., Vertical
498 characterization of highly oxygenated molecules (HOMs) below and above a boreal forest
499 canopy. *Atmospheric Chemistry and Physics* **2018,** *18*, (23), 17437-17450.
500 38.   Zaytsev, A.; Koss, A. R.; Breitenlechner, M.; Krechmer, J. E.; Nihill, K. J.; Lim, C. Y.;
501 Rowe, J. C.; Cox, J. L.; Moss, J.; Roscioli, J. R.; Canagaratna, M. R.; Worsnop, D. R.; Kroll, J.
502 H.; Keutsch, F. N., Mechanistic study of the formation of ring-retaining and ring-opening
503 products from the oxidation of aromatic compounds under urban atmospheric conditions. *Atmos*
504 *Chem Phys* **2019,** *19*, (23), 15117-15129.
505 39.   Kroll, J. H.; Donahue, N. M.; Jimenez, J. L.; Kessler, S. H.; Canagaratna, M. R.; Wilson,
506 K. R.; Altieri, K. E.; Mazzoleni, L. R.; Wozniak, A. S.; Bluhm, H.; Mysak, E. R.; Smith, J. D.;
507 Kolb, C. E.; Worsnop, D. R., Carbon oxidation state as a metric for describing the chemistry of
508 atmospheric organic aerosol. *Nature Chemistry* **2011,** *3*, 133.
509 40.   McDonald, B. C.; de Gouw, J. A.; Gilman, J. B.; Jathar, S. H.; Akherati, A.; Cappa, C. D.;
510 Jimenez, J. L.; Lee-Taylor, J.; Hayes, P. L.; McKeen, S. A.; Cui, Y. Y.; Kim, S.-W.; Gentner, D.
511 R.; Isaacman-VanWertz, G.; Goldstein, A. H.; Harley, R. A.; Frost, G. J.; Roberts, J. M.; Ryerson,
512 T. B.; Trainer, M., Volatile chemical products emerging as largest petrochemical source of urban
513 organic emissions. *Science* **2018,** *359*, (6377), 760-764.
514 41.   Guenther, A.; Hewitt, C. N.; Erickson, D.; Fall, R.; Geron, C.; Graedel, T.; Harley, P.;
515 Klinger, L.; Lerdau, M.; Mckay, W. A.; Pierce, T.; Scholes, B.; Steinbrecher, R.; Tallamraju, R.;
516 Taylor, J.; Zimmerman, P., A global model of natural volatile organic compound emissions.
517 *Journal of Geophysical Research: Atmospheres* **1995,** *100*, (D5), 8873-8892.
518 42.   Schobesberger, S.; Junninen, H.; Bianchi, F.; Lonn, G.; Ehn, M.; Lehtipalo, K.; Dommen,
519 J.; Ehrhart, S.; Ortega, I. K.; Franchin, A.; Nieminen, T.; Riccobono, F.; Hutterli, M.; Duplissy, J.;
520 Almeida, J.; Amorim, A.; Breitenlechner, M.; Downard, A. J.; Dunne, E. M.; Flagan, R. C.;
521 Kajos, M.; Keskinen, H.; Kirkby, J.; Kupc, A.; Kurten, A.; Kurten, T.; Laaksonen, A.; Mathot, S.;
522 Onnela, A.; Praplan, A. P.; Rondo, L.; Santos, F. D.; Schallhart, S.; Schnitzhofer, R.; Sipila, M.;
523 Tome, A.; Tsagkogeorgas, G.; Vehkamaki, H.; Wimmer, D.; Baltensperger, U.; Carslaw, K. S.;
524 Curtius, J.; Hansel, A.; Petaja, T.; Kulmala, M.; Donahue, N. M.; Worsnop, D. R., Molecular
525 understanding of atmospheric particle formation from sulfuric acid and large oxidized organic
526 molecules. *Proceedings of the National Academy of Sciences of the United States of America*
527 **2013,** *110*, (43), 17223-8.
528 43.   Ding, X.; Zhang, Y. Q.; He, Q. F.; Yu, Q. Q.; Wang, J. Q.; Shen, R. Q.; Song, W.; Wang,
529 Y. S.; Wang, X. M., Significant Increase of Aromatics-Derived Secondary Organic Aerosol
530 during Fall to Winter in China. *Environmental science & technology* **2017,** *51*, (13), 7432-7441.
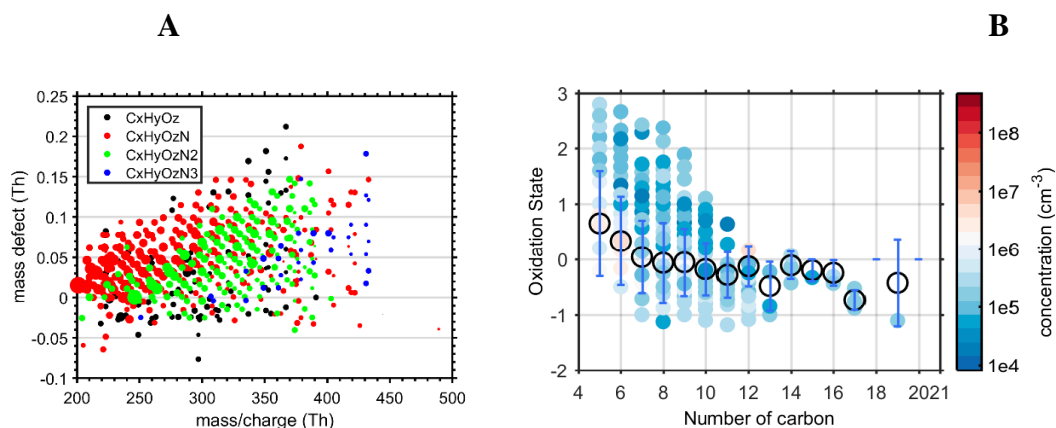531 44.   Li, M.; Zhang, Q.; Zheng, B.; Tong, D.; Lei, Y.; Liu, F.; Hong, C.; Kang, S.; Yan, L.;
532 Zhang, Y.; Bo, Y.; Su, H.; Cheng, Y.; He, K., Persistent growth of anthropogenic non-methane
533 volatile organic compound (NMVOC) emissions in China during 1990–2017: drivers, speciation
534 and ozone formation potential. *Atmos. Chem. Phys.* **2019,** *19*, (13), 8897-8913.
535 45.   Donahue, N. M.; Kroll, J. H.; Pandis, S. N.; Robinson, A. L., A two-dimensional volatility
536 basis set – Part 2: Diagnostics of organic-aerosol evolution. *Atmospheric Chemistry and Physics*
537 **2012,** *12*, (2), 615-634.

46.   Donahue, N. M.; Epstein, S. A.; Pandis, S. N.; Robinson, A. L., A two-dimensional volatility basis set: 1. organic-aerosol mixing thermodynamics. *Atmospheric Chemistry and Physics* **2011,** *11*, (7), 3303-3318.
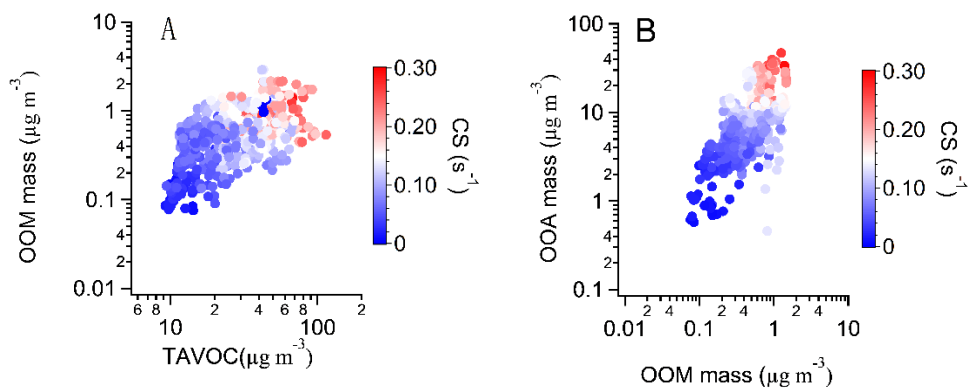
47.   Wang, J.; Ye, J.; Zhang, Q.; Zhao, J.; Wu, Y.; Li, J.; Liu, D.; Li, W.; Zhang, Y.; Wu, C.; Xie, C.; Qin, Y.; Lei, Y.; Huang, X.; Guo, J.; Liu, P.; Fu, P.; Li, Y.; Lee, H. C.; Choi, H.; Zhang, J.; Liao, H.; Chen, M.; Sun, Y.; Ge, X.; Martin, S. T.; Jacob, D. J., Aqueous production of secondary organic aerosol from fossil-fuel emissions in winter Beijing haze. *Proceedings of the National Academy of Sciences of the United States of America* **2021,** *118*, (8).

Main Figures

A   B

Figure 1. (a) **Campaign averaged OOM mass defect versus *m/z* in Beijing.** Mass defect is the difference between the exact mass and the nominal mass (the exact mass of ^{1}H is 1.007276 Da, giving a positive mass defect of 0.007276). Symbol size is proportional to the logarithm of the counting rate. Most species contain at least one N atom. (b) **Campaign averaged carbon oxidation state as a function of carbon numbers**. Black circles show mean values, with error bars showing the standard deviation. Symbol color corresponds to concentration.
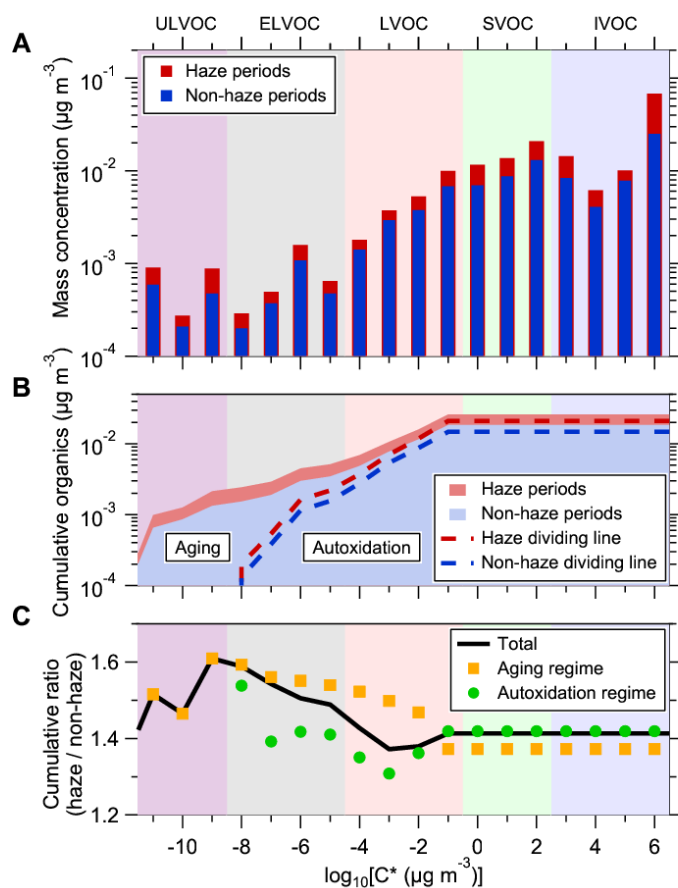
Figure 2. (a) **Scatter plot of total OOM concentration vs total aromatic VOCs (TAVOC) in Beijing during the measurement period.** Symbol color indicates the aerosol condensation sink, which correlates with the aerosol pollution level and directly controls the sink of condensable organic vapors (OOM). (b) **Scatter plot of total OOM concentration vs oxygenated organic aerosol (OOA)**. OOA is a factor resolved by positive matrix factorization (PMF) of ambient organic aerosol measured by a ToF-ACSM. These associations are likely causal, with aromatic VOC oxidation driving OOM production, and OOM condensation driving OOA formation.

601

602
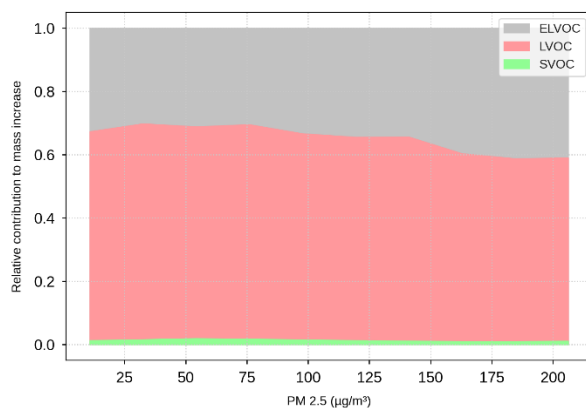
603

604

605

606

607

608

609

610

611

612

613

614

Figure 3. (a) **The summed OOM concentrations in each bin of the volatility basis set during haze (red) and non-haze (blue) periods**. The ULVOCs, ELVOCs and LVOCs have sufficiently low volatilities, and are efficient condensable material; the SVOCs contribute to particle mass via gas-particle partitioning. (b) **The cumulative OOM concentrations**. The OOMs are integrated from the lowest volatility bin to $C^* \leq 10^{0.5}$ µg m^{-3} (shaded area), indicating the tentative abundance of condensable vapors. The dashed dividing lines show volatilities estimated using two distinct VBS parameterizations to reflect the contribution of aging (multi-generation OH oxidation) and autoxidation to the OOM formation, respectively (see Method and Fig S5). (c) **The ratio of cumulative OOM concentrations during haze periods to those during non-haze periods**. The solid black line, yellow squares and green circles represent the ratio of total OOMs, OOMs in the aging regime, and OOMs in the autoxidation regime, respectively. OOMs during haze periods have a similar volatility distribution to that during non-haze periods, but with notably higher concentrations in all volatility bins. The overall increase in the tentative condensable vapors from non-haze to haze periods is approximately 40 % in mass. Further, these OOMs in the ULVOC and ELVOC ranges rise more than those in the LVOC range, with species potentially formed from aging pathways being the major contributor.
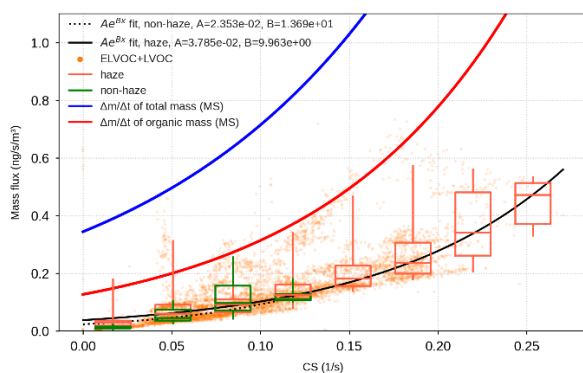
633 A

634
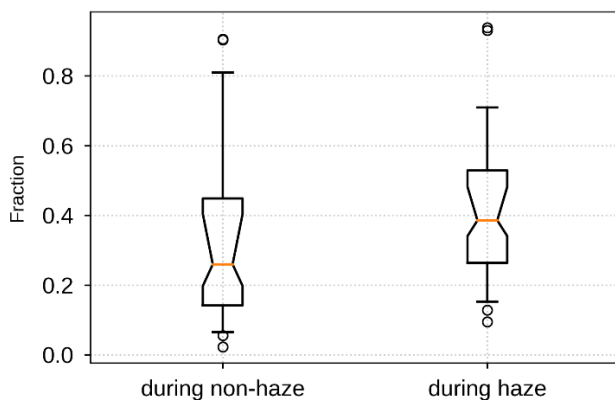
635 B

636

637 **C**

638

639 **Figure 4**. (a) The relative contributions of ELVOC, LVOC and SVOC to modeled total mass flux
640 for different PM$_{2.5}$ levels, noting that ULVOC is also included in ELVOC during the modeling.
641 Contributions are based on growth rates modeled during growth periods and measured vapor
642 concentrations. (b) The variation of total mass fluxes of ELVOC and LVOC as a function of
643 condensation sink (CS). The black solid curve and red box and whisker ranges are for PM$_{2.5}$ > 75
644 μg m^{-3} (haze periods), while the dotted curve and green box and whisker ranges are for PM$_{2.5}$ < 75
645 μg m^{-3}. The orange points represent total flux from ELVOC and LVOC. The blue and red solid

646 curve represent modeled total mass fluxes and organic mass fluxes during positive mass flux
647 events. (c) The contribution of OOM to organic aerosol mass during non-haze and haze periods.
648 The organic aerosol mass in $PM_{2.5}$ mass is measured by a ToF-ACSM, along with nitrate, sulfate,
649 ammonium and chloride.